HHS Public Access

Author manuscript

Appl Opt. Author manuscript; available in PMC 2019 January 22.

Published in final edited form as:

Appl Opt. 2019 January 10; 58(2): 428–435. doi:10.1364/AO.58.000428.

Dispersion compensation by a liquid lens (DisCoBALL)

MICHAEL E. DURST[*], **ANTHONY TURCIOS**, **COLIN LAURENCE**, and **EMMA MOSKOVITZ**

Department of Physics, Middlebury College, Middlebury, VT 05753

Abstract

We present dispersion compensation by a liquid lens (DisCoBALL), which provides tunable group-delay dispersion (GDD) that is high speed, has a large tuning range, and uses off-the-shelf components. GDD compensation is crucial for experiments with ultrashort pulses. With an electrically tunable lens (ETL) at the Fourier plane of a 4 *f* grating pair pulse shaper, the ETL applies a parabolic phase shift in space and therefore a parabolic phase shift to the laser spectrum, i.e., GDD. The GDD can be tuned with a range greater than 2×10^5 fs^2 at a rate of 100 Hz while maintaining stable coupling into a single mode fiber.

1. Introduction

Ultrafast pulsed lasers are becoming widely available [1–3], and dispersion management is essential for maintaining femtosecond pulses. While ultrafast laser systems typically incorporate a fixed amount of dispersion compensation, many applications require the dispersion to be tuned over a wide range. Optical fiber systems like fiber endoscopes require large amounts of dispersion compensation depending on their length to recover an ultrashort pulse at the output. In multiphoton microscopy (MPM), the fluorescence signal depends inversely on the excitation laser pulse width. While highly dispersive elements like acousto-optic modulators (AOMs) and high numerical aperture objective lenses can be compensated by a fixed amount of dispersion, samples of varying thickness require different amounts of dispersion compensation, particularly when imaging 3D stacks which extend from the surface to deep within biological tissue [4–6]. In an extension of MPM called temporal focusing (TF), imaging a diffraction grating onto the sample makes the excitation laser pulse width vary with depth [7–9]. Because the wavelengths are spatially dispersed, phase shifts in spectrum lead to phase shifts in space, and thus dispersion tuning shifts the temporal focus axially [10–15].

Dispersion compensation techniques typically employ angularly dispersive elements which map the spectral domain onto the spatial domain. Changing the separation of prism pairs [16,17], grating pairs [18–20], or grism pairs [21, 22] can tune the dispersion, but the tuning speed and range is limited by the mechanical translation of these elements. While non-angularly dispersive elements like dispersion compensating mirrors can generate a significant amount of dispersion through multiple reflections, tuning the dispersion can require realignment [23]. For fiber applications, the dispersion can be varied by thermally

[*]mdurst@middlebury.edu

tuned fiber-Bragg gratings [24, 25], in-fiber etalons [26], electronically driven phase modulators [27–29], and waveguide grating routers combined with external pulse shapers [30–34].

State-of-the-art dispersion compensation relies on programmable 4 f pulse shapers, consisting of a grating pair separated by a 1:1 telescope in which the spectral phase is controlled by spatial modulation in the Fourier plane [35, 36]. Electronically addressed devices such as AOMs [37], liquid crystal spatial light modulators (SLMs) [38], and deformable mirrors (DMs) [39] can create arbitrary phase profiles to compensate for higher-order dispersion. In addition, these programmable devices can simultaneously measure and compensate the dispersion in a system through mulitphoton intrapulse interference [40,41] and phase resolved interferometric modulation [42]. Unfortunately, phase shifts created by SLMs and DMs are typically limited to 2π radians, and their refresh rate can be slow. Clever techniques can improve the speed, such as scanning multiple patterns on a 2D SLM [43, 44] or modulating a digital micromirror device [45], but ultimately the ability to apply complex spectral phase profiles is unnecessary for most applications.

Group-delay dispersion (GDD), which corresponds to a parabolic spectral phase, is the lowest-order dispersion term which contributes to the broadening of an ultrashort laser pulse, and in many cases compensation of only the GDD is required [46]. To implement GDD compensation, a 4 f pulse shaper must simply create a parabolic phase shift rather than an arbitrary phase profile. A piezo bimorph mirror bends into a parabola with an applied voltage and can generate a large range of GDD, but it is unstable at high speeds [11]. Rotating a cylindrical lens creates an effective change in focal length and can tune the GDD over a large range [47], but its reliance on mechanical motion can be undesirable.

Here, we introduce dispersion compensation by a liquid lens (DisCoBALL), a method for tunable GDD compensation with an electrically tunable lens (ETL). We place the ETL at the Fourier plane of a 4 f pulse shaper (Fig. 1). The approximate parabolic shape of the ETL in space applies a quadratic phase in spectrum, and changing the focal length tunes the amount of applied GDD. Electrically tunable lenses are essentially liquid lenses encapsulated in a polymer membrane, and a voice coil changes the focal length by applying pressure at speeds up to 1 kHz [48]. ETLs have been used in many applications requiring fast focusing, including particle tracking [49], volumetric imaging [50–54], and temporal focusing [55]. To our knowledge, this is the first application of ETLs to femtosecond pulse shaping. This technique provides GDD compensation that is high speed, has a large tuning range, and uses off-the-shelf components.

2. Theory

We derive an expression for the amount of GDD applied as a function of the focal length of the ETL. Ultrashort pulses are formed when a wide bandwidth of frequencies add up in phase, but the pulse width will broaden in time as glass and other dispersive elements shift these frequencies out of phase. The spectral phase can be written as a Taylor series expansion

$$\phi(\omega) = \phi(\omega_0) + \left.\frac{d\phi}{d\omega}\right|_{\omega_0} (\omega - \omega_0) + \ldots + \frac{1}{2!}\left.\frac{d^2\phi}{d\omega^2}\right|_{\omega_0} (\omega - \omega_0)^2 + \frac{1}{3!}\left.\frac{d^3\phi}{d\omega^3}\right|_{\omega_0} (\omega - \omega_0)^3 + \ldots, \quad (1)$$

where the first two terms only shift the pulse in time. The lowest-order term which broadens the pulse is the quadratic term, and its coefficient is known as the GDD. In our 4 *f* pulse shaper, the frequencies are approximately linearly mapped to position, so we can calculate the GDD from the phase shift due to the thickness of the ETL. We let the shape of the ETL be described as a plano-convex lens of radius of curvature *R*. The phase shift for a ray passing through lateral position *x* is given by

$$\Delta\,\phi = k\,\Delta\,OPL = \frac{2\pi}{\lambda}(n-1)\left(d - R + \sqrt{R^2 - x^2}\right), \quad (2)$$

where *n* is the refractive index of the ETL material, *d* is the thickness of the ETL at its center, and *x* is the lateral distance from the center of the ETL. Ignoring constant phase terms and assuming that the focal length of the lens is large ($R \gg x$), the optical path length can be written as

$$\Delta\,\phi \approx -\frac{2\pi}{\lambda}(n-1)\frac{x^2}{2R} = -\frac{2\pi}{\lambda}\frac{x^2}{2f}, \quad (3)$$

where we have used the lens maker's formula $1/f = (n-1)/R$ for the focal length *f* of a plano-convex lens. Note that the refractive index of the lens no longer appears in our expression for $\Delta\phi$ because it is included in the focal length *f*.

For ultrashort pulses with bandwidth on the order of 10 nm, the diffraction grating equation yields an approximately linear relationship between frequency and position at the Fourier plane of the 4 *f* pulse shaper. Therefore, the position of a particular frequency is proportional to the ratio of the lens aperture diameter *D* to the total bandwidth across the aperture Ω

$$x = \left(\frac{D}{\Omega}\right)(\omega - \omega_0), \quad (4)$$

where Ω is determined by the geometry of the apparatus using the groove density of the grating and the focal length of the collimating lens. The phase shift then becomes

$$\Delta\,\phi = -\frac{2\pi}{\lambda}\left(\frac{D}{\Omega}\right)^2\frac{(\omega - \omega_0)^2}{2f}. \quad (5)$$

From Eq. 1, the GDD is related to the phase by $\Delta\phi = GDD\,(\omega - \omega_0)^2/2$, so we can express the GDD in terms of the pulse shaper geometry

$$GDD = -\frac{2\pi}{\lambda}\left(\frac{D}{\Omega}\right)^2\frac{1}{f}. \quad (6)$$

In summary, the induced GDD is determined by the focal length of the ETL, the wavelength λ, the lens aperture diameter D, and the bandwidth across the aperture Ω as determined by the diffraction grating geometry.

GDD will serve to broaden the pulse in time, and we measure the effect of GDD through changes in the pulse width. For a Gaussian pulse, the theoretical full-width-at-half-maximum (FWHM) temporal pulse width as a function of GDD is given by

$$\Delta\tau_{\text{FWHM}} = \Delta\tau_{\text{chirp-free}}\left[1 + \left(4\ln(2)\frac{GDD}{\Delta\tau^2_{\text{chirp-free}}}\right)^2\right]^{\frac{1}{2}}. \quad (7)$$

where $\Delta\tau_{\text{chirp-free}}$ is the minimum pulse width (FWHM) when the GDD is zero.

3. Experiment and Results

The DisCoBALL experimental layout is shown in Fig. 2. A laser (Spectra Physics Mai Tai) with a center wavelength of λ = 800 nm and a Gaussian spectrum with a 7.7 nm full-width-at-half-maximum (FWHM) bandwidth is incident upon a ruled reflective diffraction grating (1200 lines per mm) at an incident angle of 43°. The diffraction grating separates the beam into its individual frequency components, which are then collimated by a spherical lens (f_{col} = 20 cm) placed one focal length f_{col} away from the grating. At the Fourier plane, we place the ETL (Optotune EL-16–40-TC-VIS-20D), which is controlled by a lens driver (Gardasoft TR-CL180). For this ETL, the aperture size is D = 16 mm, the damage threshold is 10 kW / cm^2, the AR coating transmits 450 – 950 nm, and the extreme focal powers are 1 / f = ±10 diopters, i.e., the shortest possible focal lengths are f = ±0.1 m. Because the ETL membrane shape is affected by gravity, the ETL is mounted horizontally with the optical axis passing vertically through its center. The beam path is folded with two plane mirrors held at 45°. The second half of the pulse shaper is the mirror image of the first half, using an identical fixed collimating lens and diffraction grating. Before inserting the ETL into the pulse shaper, we adjust the spacing of the diffraction gratings to achieve a transform-limited pulse width. This provides constant GDD pre-compensation of other optical elements not pictured, including an optical isolator, half waveplate, and polarizing beamsplitter. Therefore, the total GDD in the system is zero when the ETL focal power is zero, and any pulse broadening is due to the ETL.

We measure the effects of the GDD on the laser pulse through second-order interferometric autocorrelation with a Michelson interferometer, using a GaAsP photodiode (Hamamatsu

G1115) as a two-photon absorption detector [56]. Autocorrelation splits the pulse into two copies with a beamsplitter and interferes it with itself. The resulting interference pattern contains information about the pulse width, which is sufficient to characterize the effects of GDD on a Gaussian pulse [57]. In Fig. 3, we present experimental and theoretical interferometric autocorrelation traces for ETL focal powers of 0.0, +1.0, and +2.0 diopters. To compare to theory, we assume a Gaussian shape in time and frequency and calculate the interferometric autocorrelation trace following Ref. [58]. We acquire the laser spectrum using a fiber-coupled spectrometer (Ocean Optics HR2000+), and the power spectrum of the laser does not change width as the spectral phase is increased (insets of Fig. 3(a)–(c)). The broadening of the pulse is characterized by the intensity autocorrelation, which is calculated by low pass filtering the interferometric data. Finally, we calculate the intensity FWHM using the deconvolution factor $\sqrt{2}$ for a Gaussian pulse [58]. In Fig. 3(b) and (c), the autocorrelation traces show the signature wings of broadening due to GDD, without signs of any higher-order-dispersion terms [57].

The temporal pulse width for different ETL focal lengths is shown in Fig. 4. We observe a transform-limited pulse width of 111 fs at 0.0 diopters (Fig. 5(b)), and the pulse width broadens to 2.59 ps at −2.0 diopters (Fig. 5(c)). We calculate the theoretical FWHM pulse width as a function of GDD using (Eq. 7) (red line in Fig. 4). The theoretical line in Fig. 4 is not a fit but rather is calculated based on the known laser parameters, optical layout, and the focal power given by the ETL controller. As shown in Fig. 4(a), the measured pulse width (blue dots) agrees well with the theoretical pulse widths (red line) over the range of −2.0 diopters to +2.0 diopters, which corresponds to the GDD range of $+1.1 \times 10^5$ fs^2 to -1.1×10^5 fs^2. Beyond this focal power, pulse width begins to diverge from theory due to the onset of spatial chirp (Fig. 4, inset), which is discussed below.

To assess the speed of the device, we apply a sinusoidal modulation of the focal power to the ETL. Rather than measure the pulse width through autocorrelation, we measure the two-photon photocurrent induced in a GaAsP photodiode, which is inversely proportional to the pulse width. In Fig. 5(a), we vary the focal length of the ETL with a 100 Hz sine curve, which was chosen due to the 7 ms response time of the ETL. Using a beamsplitter, we simultaneously measure the optical power with a Si photodiode (Thorlabs PDA36A), which has a one-photon absorption response at this wavelength, revealing <1% power fluctuation through the pulse shaper. Because the 4 f pulse shaper was aligned such that 0.0 diopters yields a minimum pulse width, the two-photon absorption signal (solid blue line) reaches a maximum every time the ETL passes through a focal power of 0.0 diopters, i.e., twice per cycle.

While this simple GDD-tuning apparatus behaves as expected, the ETL represents an additional lens in the beam path, and at large focal powers creates spatiotemporal coupling. It has been shown theoretically and experimentally that large amounts of GDD can lead to spatial chirp across the beam [59–62]. In order to investigate the spatial chirp, we couple the beam out of the DisCoBALL apparatus into a step-index single-mode fiber (SMF) with greater than 50% coupling efficiency. Any spatial chirp would be revealed by a narrowed spectrum exiting the fiber and a correspondingly wider minimum pulse width, as well as a decrease in the output power. To align the fiber, we maximize the one-photon power

throughput with the ETL set to 0.00 diopters. After passing through 1 meter of SMF (Thorlabs 780HP, 4.4 μm core), the pulse width broadens to 1.04 ps, and with the ETL tuned to 0.74 diopters, a pulse width of 117 fs is recovered (Fig. 6(b) and (c)). By simply changing the focal length of the ETL, we can compensate for several meters of fiber. The applied GDD by the ETL of -4.1×10^4 fs^2 deviates from the estimated dispersion of the SMF of 3.8×10^4 fs^2, likely due to the fiber coupling lenses adding dispersion to the beam path. Note that low powers (<1 mW) must be used with SMF due to the onset of nonlinear distortion, yielding autocorrelation traces with poor signal-to-noise ratios. At high-speed (100 Hz), the output power varies by less than 3% (Fig. 6(a)), and the laser spectrum FWHM varies by 0.5 nm. The two-photon signal in Fig. 6(a) (solid blue line) reaches a peak when the fiber dispersion is fully compensated. Due to a resonance at high speed, we observe that the focal power command sent to the ETL must be larger for the 100 Hz case (peak two-photon signal at 1.2 diopters) than the static case (peak at 0.74 diopters) in order to fully compensate for the fiber dispersion. This resonant response is discussed further in the Discussion section.

Because femtosecond pulses can lead to nonlinearities in step-index SMF at low powers due to its small core size, we demonstrate the high-speed stability of DisCoBALL at higher powers in an endlessly single-mode large-mode-area (LMA) photonic crystal fiber (NKT Photonics LMA-20, 20 μm core). After passing through 0.9 m of LMA fiber, the pulse width broadens to 884 fs, and with the ETL tuned to 0.62 diopters, a pulse width of 113 fs is recovered (Fig. 7(b) and (c)). The applied GDD by the ETL of -3.5×10^4 fs^2 agrees with the estimated dispersion of the LMA of 3.4×10^4 fs^2. In addition, we measure the output power and the laser spectrum exiting the fiber. For high-speed tuning at 100 Hz, the output power varies by less than 3% (Fig. 7(a)), and the laser spectrum FWHM varies by 0.3 nm.

4. Discussion

We have demonstrated high-speed dispersion tuning over a large GDD range. By placing an ETL at the Fourier plane of the pulse shaper, changing the focal length creates a tunable parabolic phase shift across the spectrum, effectively tuning the GDD. Despite the ETL changing focal length from infinite to ±50 cm over the ±2 diopters range, the beam pointing is stable because each individual frequency beamlet is focused at the ETL. Thus, each narrow frequency beamlet encounters a flat segment of the ETL rather than the full curvature of the lens. However, as the focal power of the ETL increases, this is no longer the case, and spatio-temporal coupling becomes an issue. Single-mode fiber coupling is therefore an essential component of this technique to eliminate spatial chirp at the output. As shown above, single-mode large-mode-area fiber allows for fiber delivery of femtosecond pulses with minimal nonlinear distortion. Also, hollow core photonic bandgap fibers support ultrashort pulses [63] by guiding light mostly in air, and these would be an excellent solution without adding additional dispersion when used at its specific zero dispersion wavelength.

For experiments in which a larger tuning range is required, several strategies can be implemented to overcome the spatial chirp. A double pass configuration can theoretically undo the spatial chirp, at the cost of poor throughput due to the two extra grating surfaces and the need for a 50:50 beamsplitter [62]. Although a quarter-wave plate combined with a polarization beamsplitter can increase the throughput, one would have to overcome the

polarization dependence of the diffraction grating efficiency. Another option would be to expand the beam incident upon the diffraction grating in order to minimize its size when passing through the ETL [60]. Ultimately, because a spherical lens of changing focal length has been added to the beam path, achieving larger GDD with shorter focal lengths unavoidably will induce spatiotemporal coupling and will distort the beam.

At high speeds, the ETL undergoes a resonance peak at 170 Hz (Fig. 8). While this frequency is faster than the response time of the ETL, this resonant response affects the focal power amplitude at all frequencies above DC. In Fig. 8, we program the ETL focal power with a sine curve with amplitude 2.0 diopters and measure the ratio of the maximum two-photon absorption signal to the minimum two-photon signal. A decrease in this two-photon ratio means that the actual focal power range and therefore the GDD range is less than the requested range. This explains our data at 100 Hz, in which we had to drive the ETL at a larger than expected focal power amplitude to compensate for each fiber, while the constant focal powers used for autocorrelations agree with the known fiber dispersion values.

There are several applications in which such a high-speed dispersion tuning device will have an immediate impact. A temporal focusing microscope requires high-speed, large-range dispersion tuning to scan the focal plane [9–11, 15]. Because this dispersion information is preserved even when transmitted through an optical fiber, the dispersion can be tuned remotely and provide axial scanning at the sample without any moving parts. Another application is in the development of long-wavelength ultrashort pulsed lasers which use soliton self-frequency shift in optical fibers [3, 64]. The wavelength of these sources is typically tuned by changing the input power, but tuning the dispersion instead will have the same effect without large changes in output power. Lastly, tunable dispersion could increase the versatility of the Talbot effect in fiber communications [28, 65, 66]. The Talbot effect can be implemented in the temporal domain to change the repetition rate of a pulse train or in the frequency domain to change the free spectral range (FSR) of a frequency comb. Current efforts involve a fixed amount of dispersion, but tuning the dispersion over a large range could greatly increase the repetition rate or FSR values available [29].

5. Conclusion

In this paper, we have demonstrated femtosecond pulse shaping with an electrically tunable lens. For applications in which only second-order dispersion compensation is required, simply changing the focal length of the ETL can rapidly change the GDD with a large tuning range. Also, this system uses only off-the-shelf components at a cost that is an order of magnitude less than systems using AOMs, SLMs, or DMs. GDD-tuning at a range over 10^5 fs^2 at 100 Hz has been achieved, and dispersion compensation of optical fiber was achieved with computer control.

Acknowledgments

Funding

Research reported in this publication was supported by an Institutional Development Award (IDeA) from the National Institute of General Medical Sciences of the National Institutes of Health under grant number

P20GM103449. Its contents are solely the responsibility of the authors and do not necessarily represent the official views of NIGMS or NIH.

References

1. Coffey V, "Ultrafast and ultrashort: some recent advances in pulsed lasers," Opt. Photonics News 25, 28–35 (2014).
2. Lefort C, "A review of biomedical multiphoton microscopy and its laser sources," J. Phys. D: Appl. Phys (2017).
3. Xu C and Wise F, "Recent advances in fibre lasers for nonlinear microscopy," Nat. Photonics 7, 875–882 (2013).
4. Kobat D, Durst ME, Nishimura N, Wong AW, Schaffer CB, and Xu C, "Deep tissue multiphoton microscopy using longer wavelength excitation," Opt. Express 17, 13354–13364 (2009). [PubMed: 19654740]
5. Horton NG, Wang K, Kobat D, Clark CG, Wise FW, Schaffer CB, and Xu C, "In vivo three-photon microscopy of subcortical structures within an intact mouse brain," Nat. Photonics 7, 205–209 (2013).
6. Sun B, Salter PS, and Booth MJ, "Effects of sample dispersion on ultrafast laser focusing," J. Opt. Soc. Am. B 32, 1272–1280 (2015).
7. Zhu G, Van Howe J, Durst M, Zipfel W, and Xu C, "Simultaneous spatial and temporal focusing of femtosecond pulses," Opt. Express 13, 2153–2159 (2005). [PubMed: 19495103]
8. Oron D, Tal E, and Silberberg Y, "Scanningless depth-resolved microscopy," Opt. Express 13, 1468–1476 (2005). [PubMed: 19495022]
9. Durst ME, Zhu G, and Xu C, "Simultaneous spatial and temporal focusing in nonlinear microscopy," Opt. Commun 281, 1796–1805 (2008). [PubMed: 18496597]
10. Durst ME, Zhu G, and Xu C, "Simultaneous spatial and temporal focusing for axial scanning," Opt. Express 14, 12243–12254 (2006). [PubMed: 19529653]
11. Straub A, Durst ME, and Xu C, "High speed multiphoton axial scanning through an optical fiber in a remotely scanned temporal focusing setup," Biomed. Opt. Express 2, 80–88 (2011).
12. He F, Zeng B, Chu W, Ni J, Sugioka K, Cheng Y, and Durfee CG, "Characterization and control of peak intensity distribution at the focus of a spatiotemporally focused femtosecond laser beam," Opt. Express 22, 9734–9748 (2014). [PubMed: 24787858]
13. Leshem B, Hernandez O, Papagiakoumou E, Emiliani V, and Oron D, "When can temporally focused excitation be axially shifted by dispersion?" Opt. Express 22, 7087–7098 (2014). [PubMed: 24664057]
14. Hernandez O, Papagiakoumou E, Tanese D, Fidelin K, Wyart C, and Emiliani V, "Three-dimensional spatiotemporal focusing of holographic patterns," Nat. Commun 7, 11928 (2016). [PubMed: 27306044]
15. Ding Y, Aguilar AC, and Li C, "Axial scanning with pulse shaping in temporal focusing two-photon microscopy for fast three-dimensional imaging," Opt. Express 25, 33379–33388 (2017).
16. Fork R, Martinez O, and Gordon J, "Negative dispersion using pairs of prisms," Opt. Lett 9, 150–152 (1984). [PubMed: 19721526]
17. Akturk S, Gu X, Kimmel M, and Trebino R, "Extremely simple single-prism ultrashort-pulse compressor," Opt. Express 14, 10101–10108 (2006). [PubMed: 19529405]
18. Martinez O, "3000 times grating compressor with positive group velocity dispersion: Application to fiber compensation in 1.3–1.6 μm region," IEEE J. Quantum Electron. 23, 59–64 (1987).
19. Zhang J, Etemad S, and Zhao JH, "Tunable dispersion compensation by an angular conserved grating–pair system," Appl. Opt 34, 6500–6505 (1995). [PubMed: 21060501]
20. Chauhan V, Bowlan P, Cohen J, and Trebino R, "Single-diffraction-grating and grism pulse compressors," J. Opt. Soc. Am. B 27, 619–624 (2010).
21. Gibson EA, Gaudiosi DM, Kapteyn HC, Jimenez R, Kane S, Huff R, Durfee C, and Squier J, "Effcient reflection grisms for pulse compression and dispersion compensation of femtosecond pulses," Opt. Lett 31, 3363–3365 (2006). [PubMed: 17072424]

22. Field JJ, Durfee CG, Squier JA, and Kane S, "Quartic-phase-limited grism-based ultrashort pulse shaper," Opt. Lett 32, 3101–3103 (2007). [PubMed: 17975610]
23. Wu J-L, Xu Y-Q, Xu J-J, Wei X-M, Chan AC, Tang AH, Lau AK, Chung BM, Shum HC, Lam EY,Wong KK, and Tsia KK, "Ultrafast laser-scanning time-stretch imaging at visible wavelengths," Light. Sci. Appl 6 (2017).
24. Dabarsyah B, Goh CS, Khijwania SK, Set S, Katoh K, and Kikuchi K, "Adjustable group velocity dispersion and dispersion slope compensation devices with wavelength tunability based on enhanced thermal chirping of fiber bragg gratings," J. Light. Technol 25, 2711–2718 (2007).
25. Ngo N, Li S, Zheng R, Tjin S, and Shum P, "Electrically tunable dispersion compensator with fixed center wavelength using fiber bragg grating," J. Light. Technol 21, 1568–1575 (2003).
26. Shu X and Sugden K, "Transmissive in-fiber fabry-perot etalons as tunable dispersion compensators and dispersion-slope compensators," Opt. Lett 28, 1897–1899 (2003). [PubMed: 14587768]
27. van Howe J and Xu C, "Ultrafast optical signal processing based upon space-time dualities," J. Light. Technol 24, 2649–2662 (2006).
28. Park Y and Azaña J, "Ultrahigh dispersion of broadband microwave signals by incoherent photonic processing," Opt. Express 18, 14752–14761 (2010). [PubMed: 20639961]
29. de Chatellus HG, Cortés LR, Schnébelin C, Burla M, and Azaña J, "Reconfigurable photonic generation of broadband chirped waveforms using a single cw laser and low-frequency electronics," Nat. Commun 9, 2438 (2018). [PubMed: 29934587]
30. Madsen C, Lenz G, Bruce A, Cappuzzo M, Gomez L, and Scotti R, "Integrated all-pass filters for tunable dispersion and dispersion slope compensation," IEEE Photonics Technol. Lett 11, 1623–1625 (1999).
31. Marom DM, Doerr CR, Cappuzzo MA, Chen EY, Wong-Foy A, Gomez L, and Chandrasekhar S, "Compact colorless tunable dispersion compensator with 1000-ps/nm tuning range for 40-gb/s data rates," J. Light. Technol 24, 237 (2006).
32. Li R, Fan W, Jiang Y, Qiao Z, Zhang P, and Lin Z, "Tunable compensation of gvd-induced fm–am conversion in the front end of high-power lasers," Appl. Opt 56, 993–998 (2017). [PubMed: 28158104]
33. Seno K, Suzuki K, Ooba N, Watanabe K, Ishii M, Ono H, and Mino S, "Demonstration of channelized tunable optical dispersion compensator based on arrayed-waveguide grating and liquid crystal on silicon," Opt. Express 18, 18565–18579 (2010). [PubMed: 20940749]
34. Sinefeld D, Ben-Ezra S, Doerr CR, and Marom DM, "All-channel tunable optical dispersion compensator based on linear translation of a waveguide grating router," Opt. Lett 36, 1410–1412 (2011). [PubMed: 21499373]
35. Martinez O, Gordon J, and Fork R, "Negative group-velocity dispersion using refraction," J. Opt. Soc. Am. A 1, 1003–1006 (1984).
36. Weiner AM, "Ultrafast optical pulse shaping: A tutorial review," Opt. Commun 284, 3669–3692 (2011).
37. Tournois P, "Acousto-optic programmable dispersive filter for adaptive compensation of group delay time dispersion in laser systems," Opt. Commun 140, 245–249 (1997).
38. Weiner AM, Leaird DE, Patel JS, and Wullert JR, "Programmable femtosecond pulse shaping by use of a multielement liquid-crystal phase modulator," Opt. Lett 15, 326–328 (1990). [PubMed: 19759797]
39. Zeek E, Maginnis K, Backus S, Russek U, Murnane M, Mourou G, Kapteyn H, and Vdovin G, "Pulse compression by use of deformable mirrors," Opt. Lett 24, 493–495 (1999). [PubMed: 18071550]
40. Lozovoy VV, Pastirk I, and Dantus M, "Multiphoton intrapulse interference. iv. ultrashort laser pulse spectral phase characterization and compensation," Opt. Lett 29, 775–777 (2004). [PubMed: 15072388]
41. Pillai RS, Boudoux C, Labroille G, Olivier N, Veilleux I, Farge E, Joffre M, and Beaurepaire E, "Multiplexed two-photon microscopy of dynamic biological samples with shaped broadband pulses," Opt. Express 17, 12741–12752 (2009). [PubMed: 19654680]

42. Wu T-W, Tang J, Hajj B, and Cui M, "Phase resolved interferometric spectral modulation (prism) for ultrafast pulse measurement and compression," Opt. Express 19, 12961–12968 (2011). [PubMed: 21747447]
43. Pearson BJ and Weinacht TC, "Note: Self-characterizing ultrafast pulse shaper for rapid pulse switching," Rev. Sci. Instruments 83, 046111 (2012).
44. Levitt JM, Katz O, and Silberberg Y, "Frequency-encoded multiplexed cars microscopy by rapid pulse shaping," J. Mod. Opt 61, 872–876 (2014).
45. Gu C, Chang Y, Zhang D, Cheng J, and Chen S-C, "Femtosecond laser pulse shaping at megahertz rate via a digital micromirror device," Opt. Lett 40, 4018–4021 (2015). [PubMed: 26368701]
46. Guild JB, Xu C, and Webb WW, "Measurement of group delay dispersion of high numerical aperture objective lenses using two-photon excited fluorescence," Appl. Opt 36, 397–401 (1997). [PubMed: 18250687]
47. Durst ME, Kobat D, and Xu C, "Tunable dispersion compensation by a rotating cylindrical lens," Opt. Lett 34, 1195–1197 (2009). [PubMed: 19370115]
48. Optotune Switzerland AG, Electrically Tunable Lens (2017).
49. Sancataldo G, Scipioni L, Ravasenga T, Lanzanò L, Diaspro A, Barberis A, and Duocastella M, "Three-dimensional multiple-particle tracking with nanometric precision over tunable axial ranges," Optica 4, 367–373 (2017).
50. Grewe BF, Voigt FF, van't Hoff M, and Helmchen F, "Fast two-layer two-photon imaging of neuronal cell populations using an electrically tunable lens," Biomed. Opt. Express 2, 2035–2046 (2011). [PubMed: 21750778]
51. Nakai Y, Ozeki M, Hiraiwa T, Tanimoto R, Funahashi A, Hiroi N, Taniguchi A, Nonaka S, Boilot V, Shrestha R et al., "High-speed microscopy with an electrically tunable lens to image the dynamics of in vivo molecular complexes," Rev. Sci. Instruments 86, 013707 (2015).
52. Lin C-Y, Lin W-H, Chien J-H, Tsai J-C, and Luo Y, "In vivo volumetric fluorescence sectioning microscopy with mechanical-scan-free hybrid illumination imaging," Biomed. Opt. Express 7, 3968–3978 (2016). [PubMed: 27867708]
53. Sato M, Motegi Y, Yagi S, Gengyo-Ando K, Ohkura M, and Nakai J, "Fast varifocal two-photon microendoscope for imaging neuronal activity in the deep brain," Biomed. Opt. Express 8, 4049–4060 (2017). [PubMed: 28966846]
54. Haslehurst P, Yang Z, Dholakia K, and Emptage N, "Fast volume-scanning light sheet microscopy reveals transient neuronal events," Biomed. Opt. Express 9, 2154–2167 (2018). [PubMed: 29760977]
55. Jiang J, Zhang D, Walker S, Gu C, Ke Y, Yung WH, and S.-c. Chen, "Fast 3-d temporal focusing microscopy using an electrically tunable lens," Opt. Express 23, 24362–24368 (2015). [PubMed: 26406641]
56. Ranka JK, Gaeta AL, Baltuska A, Pshenichnikov MS, and Wiersma DA, "Autocorrelation measurement of 6-fs pulses based on the two-photon-induced photocurrent in a gaasp photodiode," Opt. Lett 22, 1344–1346 (1997). [PubMed: 18188234]
57. Spence DE, Kean PN, and Sibbett W, "60-fsec pulse generation from a self-mode-locked ti:sapphire laser," Opt. Lett 16, 42–44 (1991). [PubMed: 19773831]
58. Diels J-C and Rudolph W, Ultrashort laser pulse phenomena (Elsevier, 2006).
59. Danailov M and Christov I, "Time-space shaping of light pulses by fourier optical processing," J. Mod. Opt 36, 725–731 (1989).
60. Paye J and Migus A, "Space–time wigner functions and their application to the analysis of a pulse shaper," J. Opt. Soc. Am. B 12, 1480–1490 (1995).
61. Wefers MM and Nelson KA, "Space-time profiles of shaped ultrafast optical waveforms," IEEE J. Quantum Electron. 32, 161–172 (1996).
62. Brinks D, Hildner R, Stefani FD, and van Hulst NF, "Beating spatio-temporal coupling: implications for pulse shaping and coherent control experiments," Opt. Express 19, 26486–26499 (2011). [PubMed: 22274233]
63. Prakash Ghimire N, Bao H, and Gu M, "Broadband excitation and collection in fiber-optic nonlinear endomicroscopy," Appl. Phys. Lett 103, 073703 (2013).

64. Wang K, Horton NG, Charan K, and Xu C, "Advanced fiber soliton sources for nonlinear deep tissue imaging in biophotonics," IEEE J. Sel. Top. Quantum Electron. 20, 50–60 (2014).

65. Maram R, Van Howe J, Li M, and Azana J, "Noiseless intensity amplification of repetitive signals by coherent addition using the temporal talbot effect," Nat. Commun 5, 5163 (2014). [PubMed: 25319207]

66. Cortés LR, de Chatellus HG, and Azaña J, "On the generality of the talbot condition for inducing self-imaging effects on periodic objects," Opt. Lett 41, 340–343 (2016). [PubMed: 26766709]

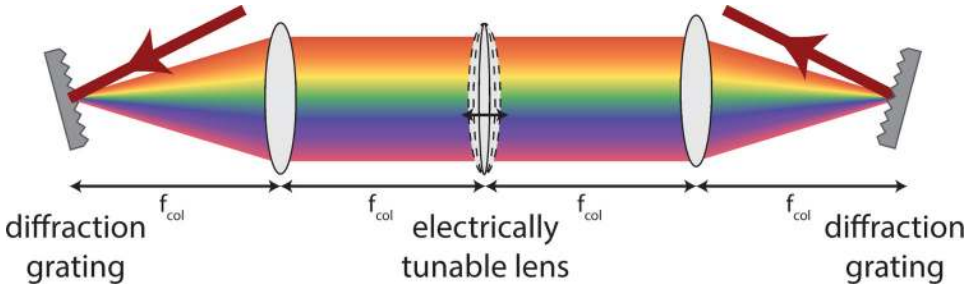

Fig. 1.

DisCoBALL GDD compensation device consisting of a 4 *f* grating pair pulse shaper with an electrically tunable lens (ETL) at the Fourier plane. Changing the focal length of the ETL tunes the GDD.

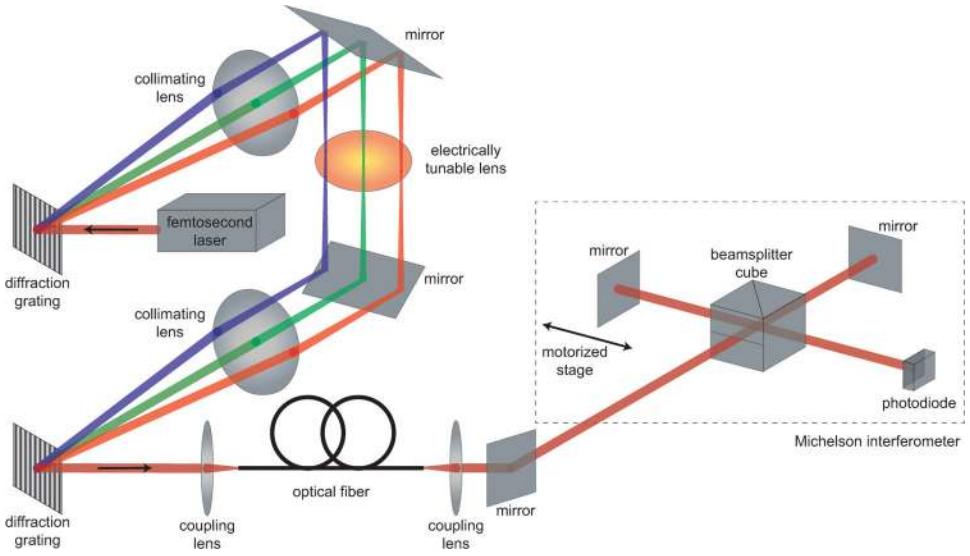

Fig. 2.

Perspective view of DisCoBALL GDD compensation device, showing folded pulse shaper geometry with vertical beam path through the ETL. After exiting the pulse shaper, the beam passes through an optional fiber coupling system. Lastly, we measure second-order autocorrelation traces using a Michelson interferometer consisting of a beamsplitter, a fixed mirror, and a mirror on a motorized linear stage.

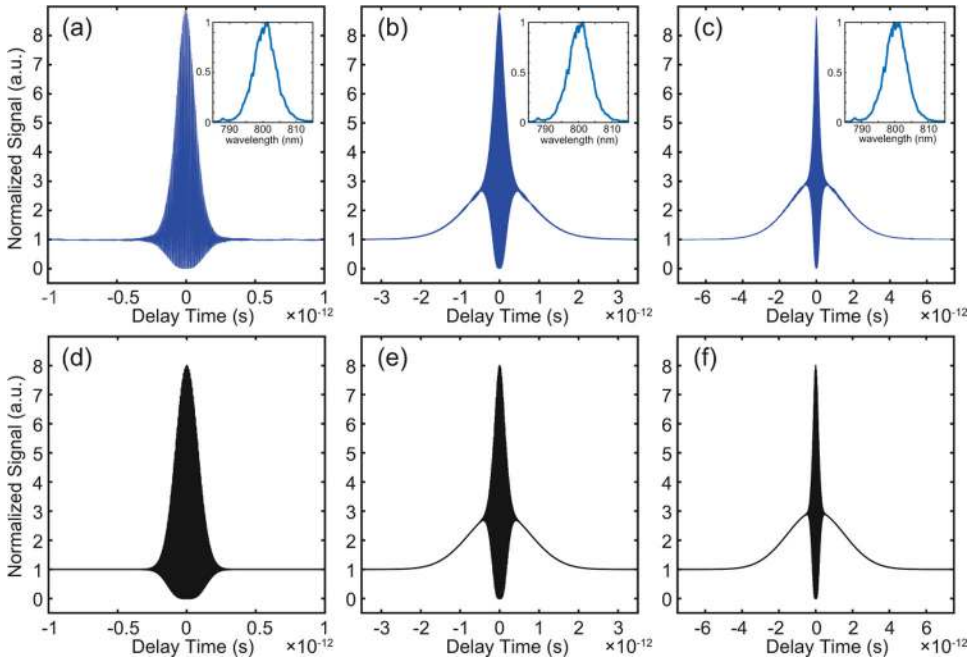

Fig. 3.

Experimental and theoretical interferometric autocorrelation traces for different ETL focal powers. (a)–(c) Experimental interferometric autocorrelation data for (a) 0.0 diopters, (b) 1.0 diopters, and (c) 2.0 diopters. Insets: Experimental power spectrum for each ETL focal power. (d)–(f) Theoretical interferometric autocorrelation plots for the same ETL focal powers of (d) 0.0 diopters, (e) 1.0 diopters, and (f) 2.0 diopters. The pulse width is calculated from the deconvolution of the intensity autocorrelation, yielding experimental pulse widths of (a) 111 fs, (b) 1.24 ps, (c) 2.41 ps, which correspond well to the theoretical widths of (d) 122 fs, (e) 1.29 ps, and (f) 2.56 ps.

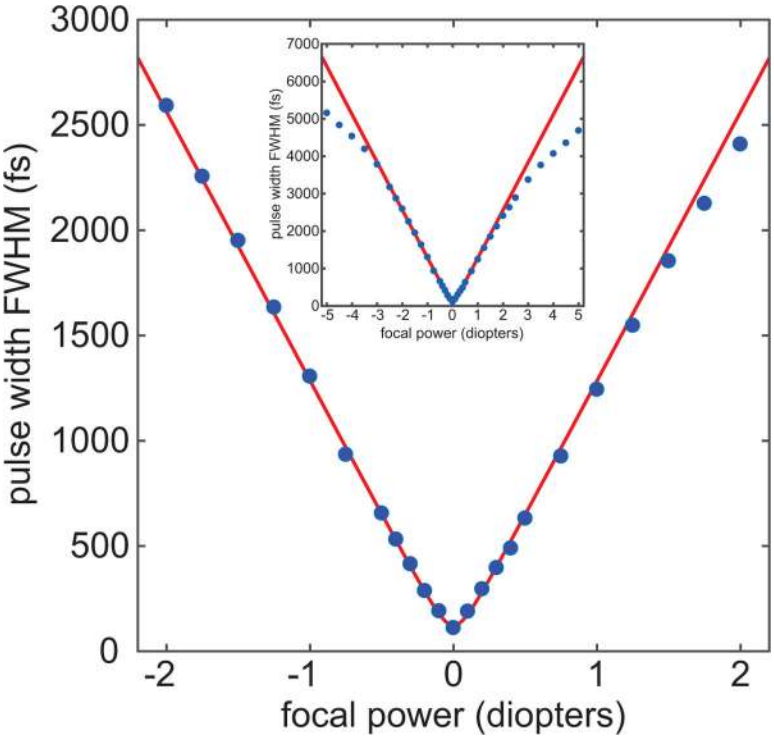

Fig. 4.

Pulse width versus focal power of the ETL. The focal power range of −2.0 diopters to +2.0 diopters corresponds to the GDD range of $+1.1 \times 10^5$ fs^2 to -1.1×10^5 fs^2. Dots represent intensity FWHM from the deconvolution of the intensity autocorrelation data. Solid curve represents theoretical Gaussian pulse width based on Eq. (7). Inset: Pulse widths measured over a wider focal power range begin to deviate from theoretical curve due to spatial chirp.

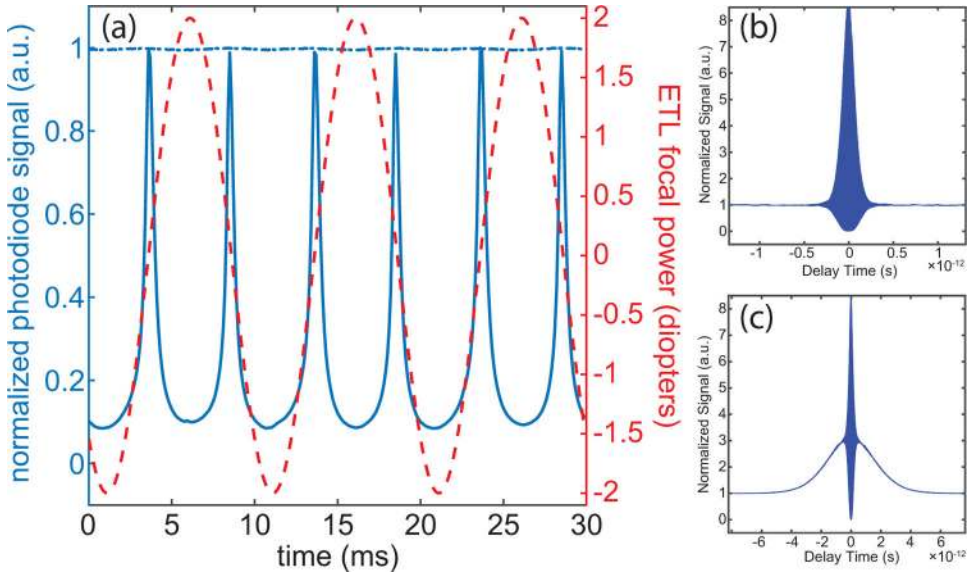

Fig. 5.

High-speed dispersion tuning with the ETL in free space. The one-photon photodiode signal (dash-dot blue line) shows a power fluctuation of 0.8%. The ETL focal power (red dashed curve) oscillates sinusoidally between −2.0 and +2.0 diopters at 100 Hz. The two-photon photodiode signal is the solid blue line, showing a peak in signal (minimum in pulse width) twice per cycle as the system's total dispersion goes through a minimum. Sample autocorrelations show (b) a transform limited pulse width of 111 fs at 0.0 diopters and (c) a chirped pulse width of 2.59 ps at −2.0 diopters.

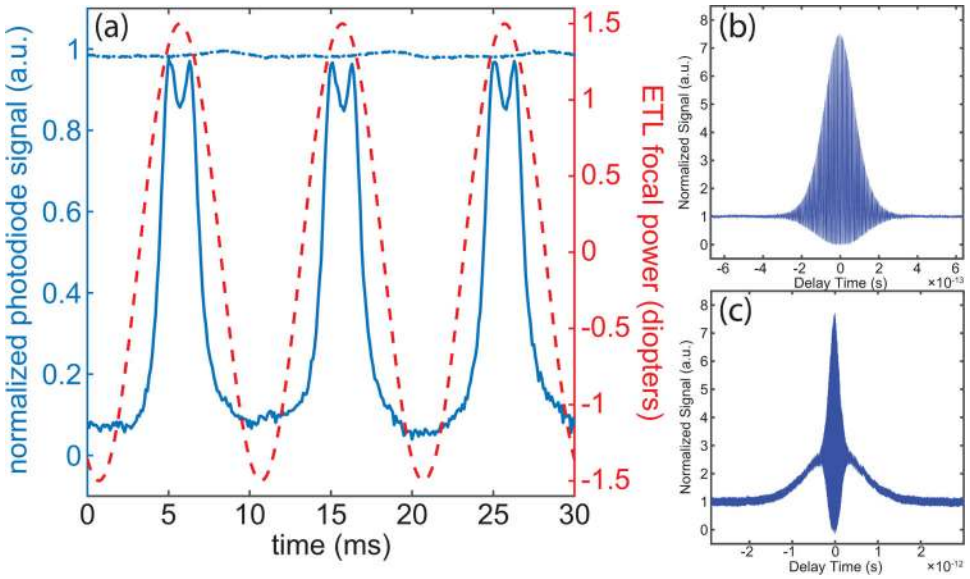

Fig. 6.

High-speed dispersion tuning through 1 m of step-index single-mode optical fiber. (a) The ETL focal power (red dashed curve) oscillates sinusoidally between −1.5 and +1.5 diopters at 100 Hz. The power coupled through the fiber is measured by the one-photon photodiode signal (dash-dot blue line), showing a power fluctuation of 2.4%. The two-photon photodiode signal (solid blue line) shows a peak in signal twice per cycle as the GDD tuning compensates for the dispersion due to the 1 m length of SMF. Sample autocorrelations in the static regime show the pulse width out of the fiber (b) with compensation and (c) without compensation. After passing through 1 m of fiber, the pulse width broadens to 1.04 ps in (c), and with the ETL tuned to 0.74 diopters, a pulse width of 117 fs is recovered in (b). Low power (1 mW) is used to avoid nonlinearities in the SMF, leading to significant noise.

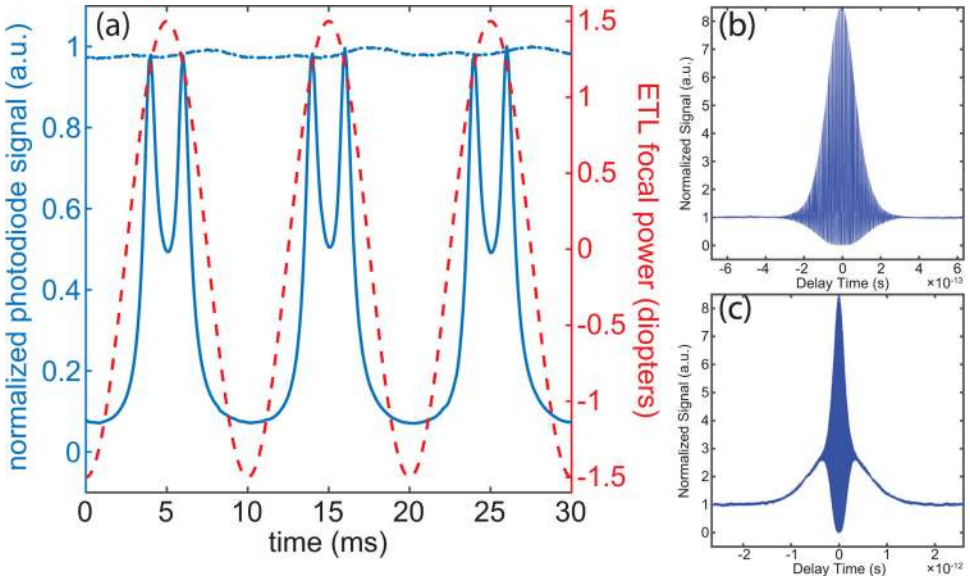

Fig. 7.

High-speed dispersion tuning through 0.9 m of large-mode-area fiber. (a) The ETL focal power (red dashed curve) oscillates sinusoidally between −1.5 and +1.5 diopters at 100 Hz. The power coupled through the fiber is measured by the one-photon photodiode signal (dash-dot blue line), showing a power fluctuation of 3%. The two-photon photodiode signal (solid blue line) shows a peak in signal twice per cycle as the GDD tuning compensates for the dispersion due to the 0.9 m length of LMA fiber. Sample autocorrelations in the static regime show the pulse width out of the fiber (b) with compensation and (c) without compensation. After passing through 0.9 m of LMA fiber, the pulse width broadens to 884 fs in (c), and with the ETL tuned to 0.62 diopters, a pulse width of 113 fs is recovered in (b).

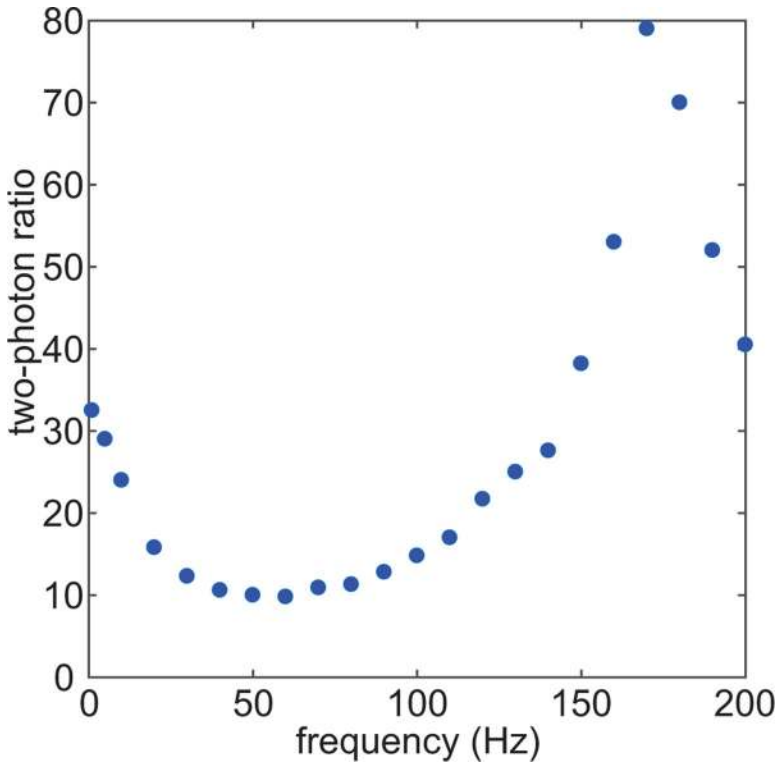

Fig. 8.

Frequency response of the ETL. The ratio of the maximum two-photon absorption signal to the minimum two-photon signal is shown when the ETL is driven by a sine curve with 2.0 diopters amplitude at various frequencies. A resonance occurs at about 170 Hz, with damping exhibited between 0 and 150 Hz.